Ceramics International 44 (2018) 5453–5458

Contents lists available at ScienceDirect

Ceramics International

journal homepage: www.elsevier.com/locate/ceramint

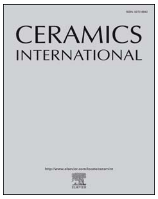

A new low-temperature firable 0.95Pb(Zr_xTi_{1-x})O_3-0.05Bi($Mn_{1/2}Ti_{1/2}$)O_3 ceramic for high-power applications

Bo Zhang, He Qi, Ruzhong Zuo*

Institute of Electro Ceramics & Devices, School of Materials Science and Engineering, Hefei University of Technology, Hefei 230009, PR China

ARTICLE INFO

Keywords:
Piezoelectric ceramics
High-power application
Low-temperature sintering
Morphotropic phase boundary
Defect dipole

ABSTRACT

A new ternary solid-solution piezoelectric ceramic of 0.95Pb(Zr_xTi_{1-x})O_3−0.05Bi($Mn_{1/2}Ti_{1/2}$)O_3 (x = 0.49–0.55) was successfully prepared via a conventional solid-state reaction. The crystal structure was found to gradually transform from tetragonal to rhombohedral phases with increasing the Zr/Ti ratio. A morphotropic phase boundary was realized in the proximity of x = 0.51, which exhibited optimum electromechanical properties of d_{33} = 275 pC/N, $\varepsilon_{33}{}^T/\varepsilon_0$ = 1226, k_p = 0.53, Q_m = 1164, tanδ = 0.66% and T_c = 341 °C as sintered at a relatively low temperature of 1120 °C. Compared with typical Pb-based complex perovskites such as Pb($Mn_{1/3}Nb_{2/3}$)O_3 and Pb($Mn_{1/3}Sb_{2/3}$)O_3, the substitution of Bi($Mn_{1/2}Ti_{1/2}$)O_3 provides obvious advantages in both sintering temperature and raw material cost. The achievement of piezoelectric and electromechanical properties was interpreted by means of a typical model concerning the interaction between defect dipoles and domains through comparative experiments. The desirable properties of the studied material system suggest a great potential for high-power device applications.

1. Introduction

Pb(Zr,Ti)O_3 (PZT)-based ternary or quaternary piezoelectric ceramics have become indispensable functional materials as actuators, ultrasonic motors and transducers [1–3]. In order to meet the requirement of the miniaturization and high power in practice, the piezoelectric ceramics are necessary to exhibit high electromechanical coupling factor (k_p), mechanical quality factor (Q_m), piezoelectric constant (d_{33}), Curie temperature (T_c) and low loss values.

Until now, a lot of attempts have been made to improve electromechanical properties of PZT based materials [4–7]. However, high Q_m, k_p and d_{33} are not easily obtained simultaneously. The most widely used method to satisfy the above-mentioned requirement is to introduce acceptor dopants in soft base materials [4–6], such as the substitution of Fe^{3+} ions for Zr^{4+}/Ti^{4+} sites in PZT by forming acceptor-oxygen vacancy defect dipoles ($Fe'_{Zr,Ti} - V_O^{\bullet\bullet}$). Another main method is via adding perovskites with B-site multivalence ions [8,9], for example, Pb($Mn_{1/3}Nb_{2/3}$)O_3 (PMN) or Pb($Mn_{1/3}Sb_{2/3}$)O_3 (PMS), to form the pinning of the domain walls by means of oxygen vacancies as a result of coexisting Mn^{2+}/Mn^{3+} ions during high-temperature sintering [10,11]. Unfortunately, the above composition systems usually need higher sintering temperature than 1250 °C. It is rather difficult to obtain ceramics based on them with excellent piezoelectric and electromechanical properties and lower sintering temperatures suitable for the application of multilayer piezoelectric devices [10,11]. In addition, the production cost would be also obviously increased owing to the usage of Nb_2O_5 and Sb_2O_3.

Bi-based perovskites compounds possess good ferroelectric properties and high T_c [12–14]. In addition, the introduction of Bi-based perovskites into PZT would have a positive effect on the decrease of the sintering temperature [15]. Bi($Mn_{1/2}Ti_{1/2}$)O_3 (BMT) would be expected to play the same role as PMN and PMS as mentioned. The effect of the BMT addition on the densification and electrical properties of PZT ceramics has never been reported in the literatures. In this work, a new ternary solid solution ceramic of BMT-PZT was prepared by a traditional mixed-oxide route with a special focus on the variation of dielectric, ferroelectric and electromechanical properties of the ternary system.

2. Experimental procedure

The 0.95PZ_xT_{1-x}−0.05BMT (x = 0.49–0.55) ceramics were prepared by a conventional solid-state reaction method using analytic-grade Bi_2O_3, PbO, ZrO_2, TiO_2 and MnO_2 as raw materials. Stoichiometric amounts of raw powders were weighed and ball-milled in alcohol with ZrO_2 balls for 6 h. The resultant mixture was dried after calcination at 850 °C for 2 h in air. The calcined powers were milled again with 5 wt% PVA as a binder for 10 h and subsequently pressed

---

* Corresponding author.
E-mail address: rzzuo@hotmail.com (R. Zuo).

https://doi.org/10.1016/j.ceramint.2017.12.178
Received 14 December 2017; Received in revised form 23 December 2017; Accepted 25 December 2017

into disk samples with a diameter of 10 mm. The specimens were heated at 550 °C for 4 h to burn out the binder, and then sintered at 1100–1150 °C for 2 h in air. In order to prevent the vaporization of Bi and Pb, sample disks were buried in the sacrificial powder of the same composition. Silver paste was painted on both sides of the disks and fired at 550 °C. The samples naturally cooled to room temperature in the furnace after sintering were marked as "furnace-cooled samples", while the samples achieved by a water-quenching process were marked as "quenched samples". The specimens were poled in a silicone oil bath at different temperatures under a dc field of 5 kV/mm for 15 min.

The bulk densities of the sintered ceramics were measured by the Archimedes method. The crystal structure of the fired ceramics was identified via an X-ray diffractometer (XRD, D/Max2500 V, Rigaku, Japan) using Cu Kα radiation. The dielectric properties were measured at 1 kHz using an LCR meter (Agilent E4980A, Santa Clara, CA) in a temperature range of 25–500 °C. The quasi-static d_{33} was measured by a Belincourt-meter (YE2730A, Sinocera, Yangzhou, China). The k_p and Q_m values were determined by a resonance-antiresonance method with an impedance analyzer (PV70A, Beijing Band ERA Co. Ltd. Beijing, China). The microstructure of the sintered samples was observed using a field-emission scanning electron microscope (FE-SEM, SU8020, JEOL, Tokyo, Japan). Before the SEM observation, samples were carefully polished and then thermally etched at 950 °C for 30 min. The polarization versus electric field (P-E) were measured using a ferroelectric test system (Precision multiferroelectric; Radiant Technologies Inc, Albuquerque, New Mexico).

3. Results and discussion

Fig. 1(a) shows the densification behavior of a few representative $0.95PZ_xT_{1-x}-0.05BMT$ compositions as a function of sintering temperature. With an increase of sintering temperature, the relative density of all three samples firstly increases up to their respective maximum values (> 96%) at 1120 °C, and then decreases with further increasing sintering temperature. Fig. 1(b)-(d) show the microstructure of $0.95PZ_xT_{1-x}-0.05BMT$ ceramics sintered at 1120 °C. It can be seen that all samples are well compacted without any obvious pores. With increasing the Zr/Ti ratio, the grain size remains almost unchanged (~ 2 μm in average). Compared with traditional PZT-based ceramics, the optimum sintering temperature of the studied material system is lowered by almost 150 °C possibly as a result of the existence of the Bi element [15]. It will exhibit larger potentials in further reducing the sintering temperature in future for applications where a much lower sintering temperature than 1000 °C is needed.

Fig. 2(a) indicates the XRD patterns of $0.95PZ_xT_{1-x}-0.05BMT$ samples as a function of x. All diffraction peaks could be well indexed to a single perovskite structure without any secondary phases, indicating that Bi^{3+} and $(Mn_{1/2}Ti_{1/2})^{3+}$ have fully diffused into the lattice and formed solid solutions with PZT. In addition, the crystal structure is found to evolve from a typical tetragonal (T) phase to a rhombohedral (R) phase with increasing x, as evidenced by the variation of the (200) diffraction lines. With increasing x, the split (200) diffraction peaks gradually merge into a single one, as shown in Fig. 2(b). In order to quantitatively analyze the evolution of the phase structure, the (200) diffraction peak profiles were fitted by using a pseudo-Voigt peak shape function, as shown in Fig. 2(c). The relative content of T (F_T) and R (F_R) phases was roughly calculated, as shown in Fig. 2(d). It is evident that a morphotropic phase boundary (MPB) between R and T phases exists in the composition range of $0.50 < x < 0.54$.

Fig. 3 displays the temperature dependent dielectric permittivity (ε_r) and loss tangent (tanδ) at 1 kHz for $0.95PZ_xT_{1-x}-0.05BMT$ ceramics. A sharp dielectric peak corresponding to the ferroelectric-paraelectric phase transition can be observed on each permittivity and loss curve. The temperature at the dielectric maxima is found to become lower from 350 °C at $x = 0.49$–331 °C at $x = 0.54$.

Fig. 4(a) shows P-E hysteresis loops as a function of poling temperature for the $x = 0.51$ sample, which was cooled to room temperature in furnace and then electrically poled under 5 kV/mm at

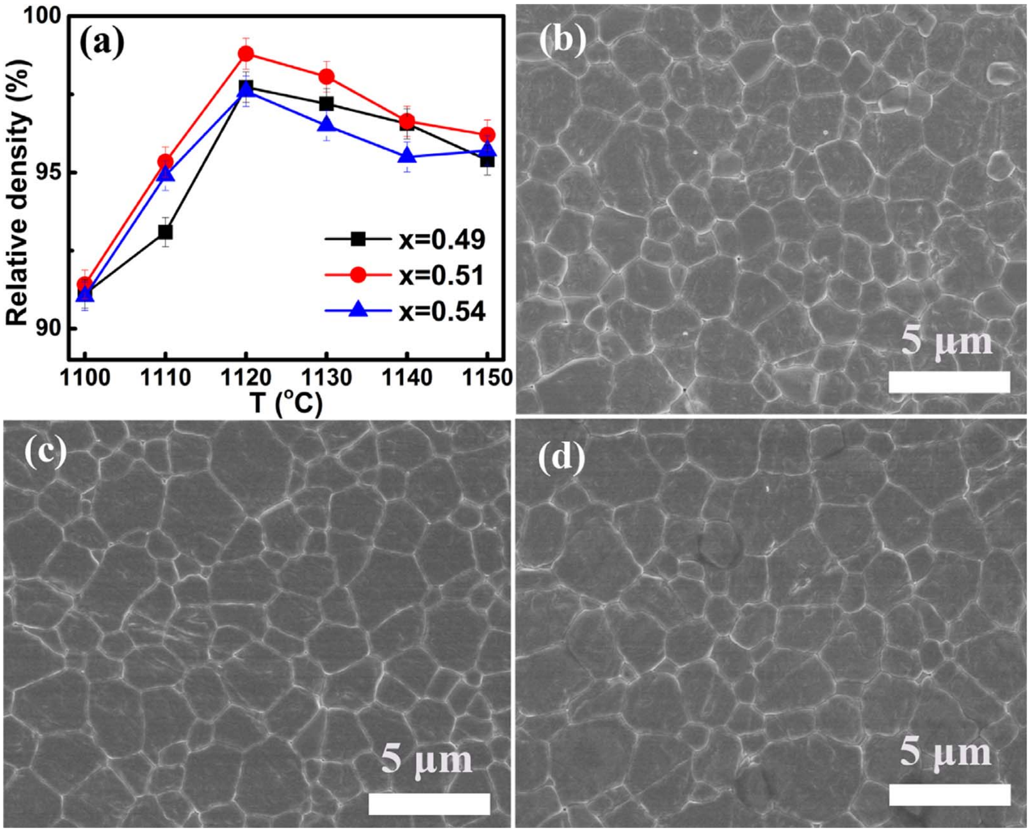

Fig. 1. (a) The variation of the relative density as a function of sintering temperature for three representative compositions, and SEM images on polished and thermally etched surfaces of $0.95PZ_xT_{1-x}-0.05BMT$ ceramics with (b) $x = 0.49$, (c) $x = 0.51$ and (d) $x = 0.54$.

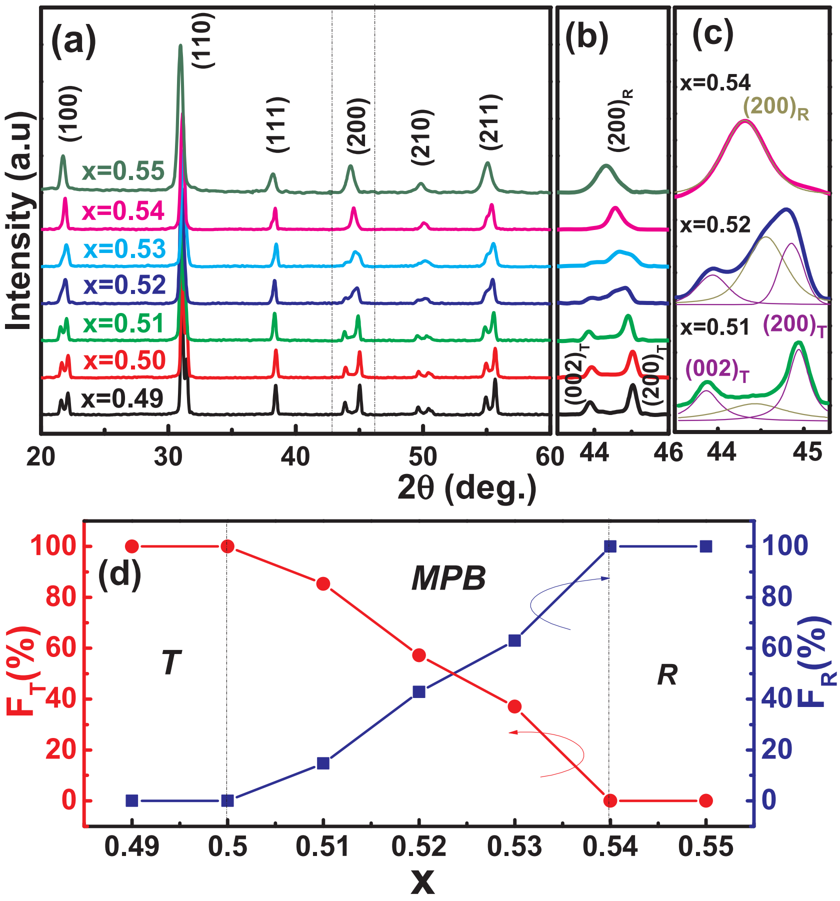

Fig. 2. (a) Room-temperature XRD patterns of $0.95PZ_xT_{1-x}-0.05BMT$ ceramics, (b) locally enlarged diffraction peaks in the 2θ range of 43°–46°, (c) peak fitting plots for the representative compositions with $x = 0.51$, 0.52 and 0.54, and (d) the variation of F_R and F_T with x.

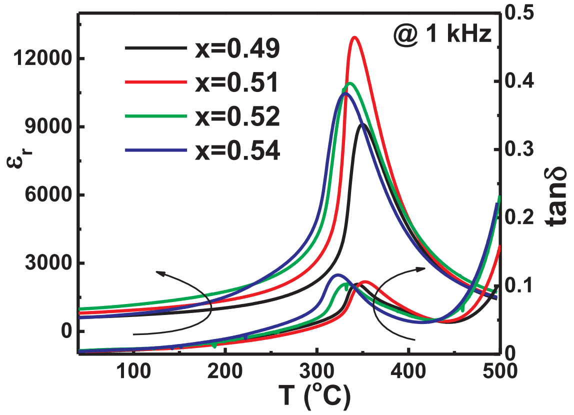

Fig. 3. Dielectric permittivity and loss tangent values at 1 kHz as a function of temperature for a few $0.95PZ_xT_{1-x}-0.05BMT$ ceramics.

different temperatures. The result indicates that poling process shows an obvious effect on the polarization switching. The aligned domain would return to its initial state after removing the electric field if the poling condition is not appropriate. As a result, little piezoelectric response would be detected, as indicated by the neglectable remanent polarization (P_r) on the pinched P-E loop in Fig. 4(a). The P-E loops gradually become asymmetric with increasing poling temperature, indicating the presence of an internal bias field along the direction of the poling electric field. This can be further reflected by the variation of piezoelectric properties measured at room temperature with increasing poling temperature, as shown in Fig. 4(b). When the poling temperature increases from 30 °C to 150 °C, the $\varepsilon_{33}{}^T/\varepsilon_0$, d_{33}, k_p, and Q_m increased from 857 to 1226, 80 to 275 pC/N, 0.23 to 0.53, and 870 to 1164, respectively. Obviously, the piezoelectric response increases drastically when an obvious asymmetric P-E loop appears, indicating highly textured domains and the formation of defect dipoles along the electric field direction. Moreover, more highly textured domains achieved with increasing poling temperatures would lead to larger maximum polarization (P_{max}) values, as shown in Fig. 4(a). When the poling temperature is above 150 °C, the values of $\varepsilon_{33}{}^T/\varepsilon_0$, d_{33}, k_p and Q_m keep almost constant with further increasing poling temperature, suggesting a sufficiently poled state above 150 °C for this system.

Fig. 5 shows the dielectric, piezoelectric and electromechanical properties of furnace-cooled $0.95PZ_xT_{1-x}-0.05BMT$ ceramics. It can be seen that $\varepsilon_{33}{}^T/\varepsilon_0$, tanδ, d_{33} and k_p values increase firstly with increasing x and reach their maximum values ($\varepsilon_{33}{}^T/\varepsilon_0 = 1226$, tanδ = 0.66%, $d_{33} = 275$ pC/N, $k_p = 0.53$) at $x = 0.51$, and then decline with further increasing x. It can be realized that the optimum electrical properties appear on the T phase-rich side within MPB. However, the variation of Q_m presents an opposite trend with increasing x and the minimum Q_m of 1164 was obtained at $x = 0.51$, because the domain wall motion becomes easier at the phase boundary. Nevertheless, excellent dielectric and piezoelectric properties of the $x = 0.51$ sample are comparable with traditional hard piezoelectric ceramics [16–18], suggesting that it should be also suitable for high-power applications.

Fig. 6(a),(b) show P-E loops for furnace-cooled and quenched samples, respectively. It can be seen from Fig. 6(a) that all the studied compositions exhibit similar double (pinched) P-E loops at room temperature as a result of a reversible switching of domains as they are electrically and/or elastically pinned by the defect dipoles, such as $Mn'_{Zr,Ti} - V_O^{\bullet\bullet}$. By comparison, saturated and symmetric P-E loops can be achieved for all the studied samples, which were water-quenched from 550 °C (> T_c), as shown in Fig. 6(b). Moreover, a larger P_r than that of the furnace-cooled (Fig. 6(a)) and poled (Fig. 4(a)) samples was obtained for quenched samples. Appropriate piezoelectric properties could be detected just after the measurement of the P-E loop for the

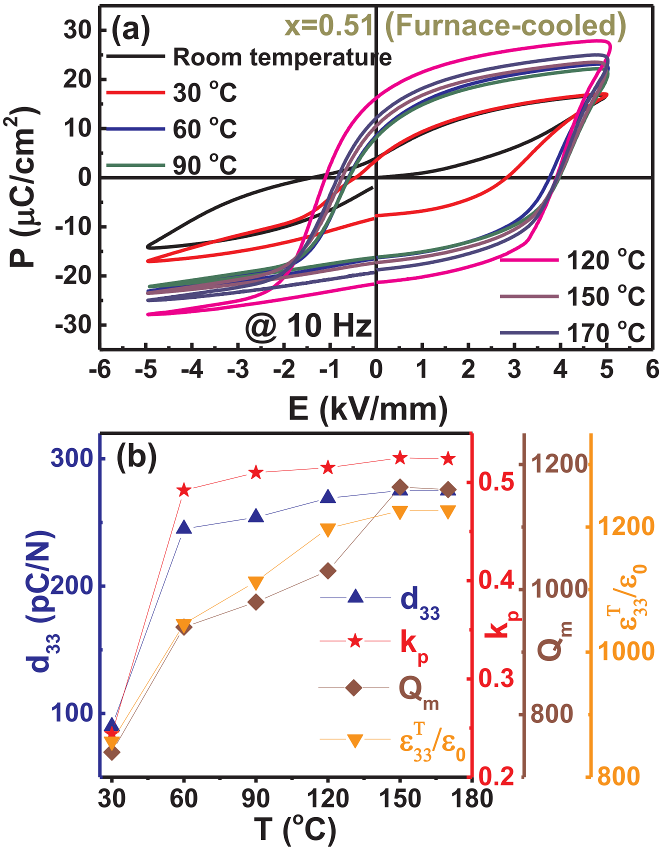

Fig. 4. (a) P-E loops and (b) d_{33}, k_p, Q_m and $\varepsilon_{33}{}^T/\varepsilon_0$ for furnace-cooled samples with $x = 0.51$ poled under 5 kV/mm at different temperatures.

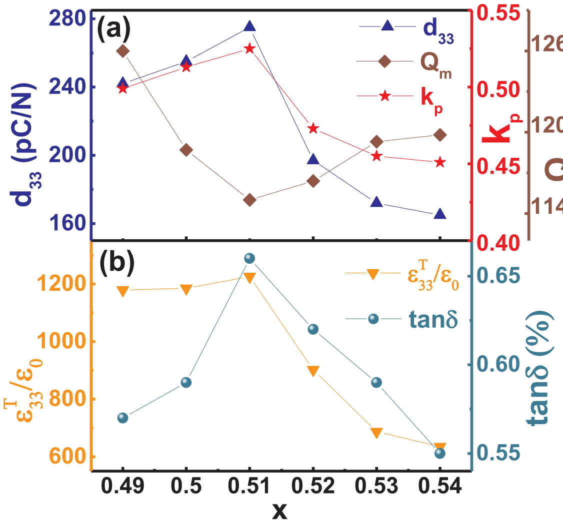

Fig. 5. Room-temperature (a) d_{33}, k_p, Q_m, (b) $\varepsilon_{33}{}^T/\varepsilon_0$ and tanδ values for the furnace-cooled $0.95PZ_xT_{1-x}-0.05BMT$ ceramics after being poled under 5 kV/mm at 150 °C for 15 min.

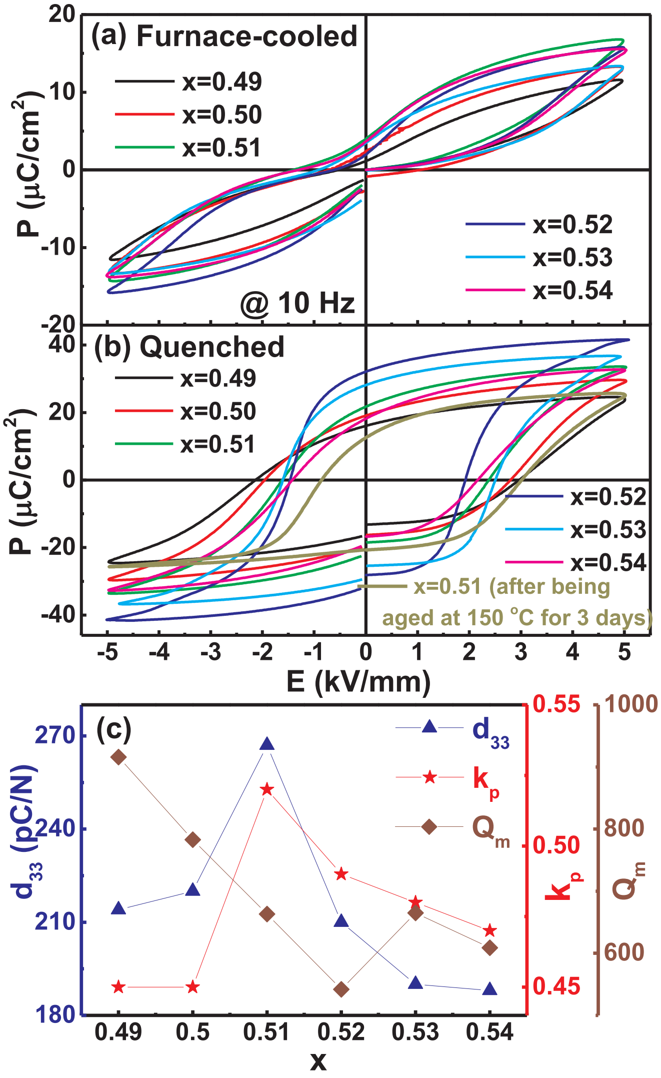

Fig. 6. Room-temperature P-E loops for the (a) furnace-cooled and (b) quenched $0.95PZ_xT_{1-x}-0.05BMT$ ceramics as well as the quenched $x = 0.51$ sample which suffered from aging at 150 °C for 3 days after electric field cycling, and (c) composition dependence of d_{33}, k_p and Q_m values after the measurement of the P-E loop for the quenched samples.

quenched samples, as shown in Fig. 6(c). This phenomenon is quite different from that observed in furnace-cooled samples, which need to be poled at high temperatures, as shown in Fig. 4. The d_{33} values achieved in quenched samples (Fig. 6(c)) are approximately equal to that of the furnace-cooled samples after being poled at 150 °C (see Fig. 5(b)), however, much smaller Q_m values are achieved for the quenched samples after electric cycling. However, after aging at 150 °C for 3 days, the Q_m value for the quenched sample increases and approximates to the value of the corresponding poled sample (Fig. 5). This can be clearly confirmed by the corresponding P-E loop of the quenched sample which was first subjected to electric field cycling and then being aged at 150 °C for 3 days, as shown in Fig. 6(b). An obviously asymmetric P-E loop indicates the presence of an internal bias field along the direction of the poling electric field.

A schematic illustration was proposed to explain the polarization response during the application of an electric field for the $x = 0.51$ ceramic with different initial states, as shown in Fig. 7. As known, the defect dipoles should randomly distribute in the paraelectric phase above T_c, as shown in Fig. 7(a). The randomly distributed defect dipoles would be frozen in the domains after water-quenching. Therefore, the direction of defect dipoles is inconsistent with that of the polarization vector, such that the domains would switch freely in accordance with the applied field (Fig. 7(b1)-(b3)), resulting in typical ferroelectric feature with a saturated P-E loop (Fig. 6(b)). Even though good piezoelectric response can be achieved in the quenched sample after electric cycling, a relatively low Q_m was achieved owing to its fragile domain state. However, randomly orientated defect dipoles are in a metastable state below T_c. The defect dipole formed between ions (Mn^{2+}/Mn^{3+}) and O^{2-} vacancies tends to align along the spontaneous polarization direction gradually, and its symmetry would be consistent

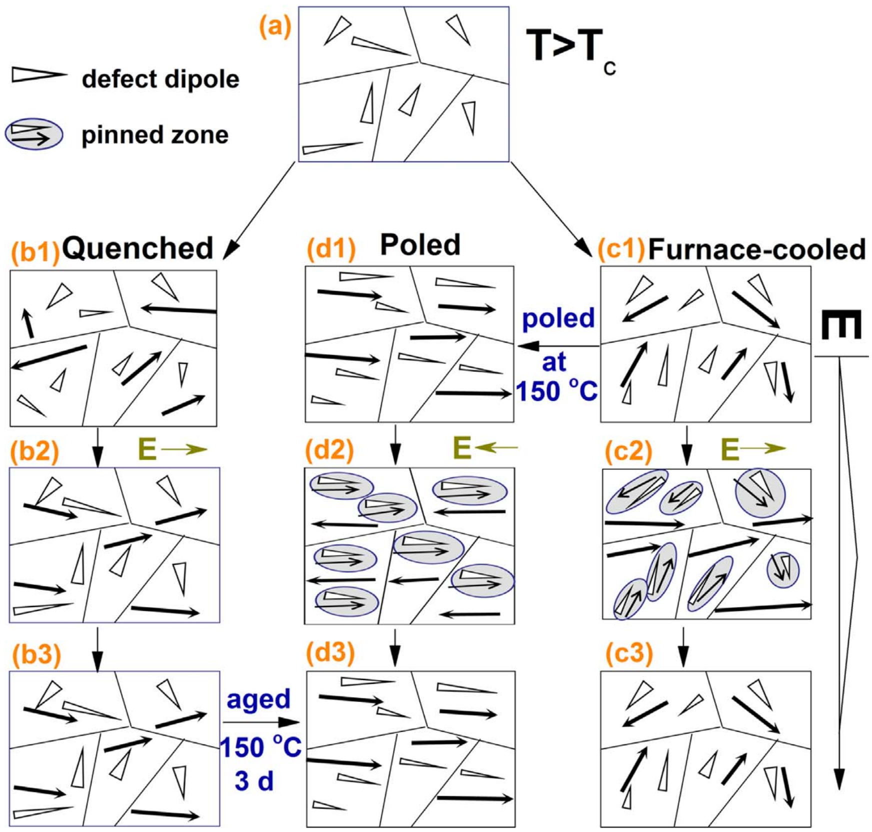

Fig. 7. A schematic illustration for the defect dipole and domain response during electric field cycling.

with the crystal symmetry during a slow cooling process (Fig. 7(c1)) or an aging process (such as Fig. 7(b3) to (d3)) [19,20], causing a pinning effect on the domains. Accordingly, the defect dipoles provide a restoring force to switch back the domains after the electric field is removed (Fig. 7(c1)-(c3)), inducing a pinched P-E loop. Both of the domains and defect dipoles align along the electric field direction during the poling process at high temperatures (Fig. 7(d1)-(d3)), resulting in a stably textured polarization state. Therefore, excellent piezoelectric properties as well as high Q_m value are achieved simultaneously.

4. Conclusions

A new low-temperature firable $0.95PZ_xT_{1-x}-0.05BMT$ piezoelectric ceramic was studied in terms of the microstructure, phase structure, dielectric, piezoelectric and ferroelectric properties. The ternary solid solution ceramics can be well densified at a relatively low temperature of ~ 1120 °C, which is about 150 °C lower than that of traditional PZT-based high-power piezoelectric ceramics. A gradual evolution from ferroelectric T phase to R phase was found with enhancing Zr/Ti ratio. Optimum dielectric and electromechanical properties of $d_{33} = 275$ pC/N, $\varepsilon_{33}^T/\varepsilon_0 = 1226$, $k_p = 0.53$, $\tan\delta = 0.66\%$, $Q_m = 1164$ and $T_c = 341$ °C were achieved in the MPB composition with $x = 0.51$. The effect of poling conditions on the piezoelectric and electromechanical properties was explained by means of the interaction model between the defect dipole and polarization vector. The experimental results suggest that $0.95PZ_xT_{1-x}-0.05BMT$ piezoelectric ceramics should have a great potential for high-power applications.

Acknowledgements

This work was supported by the National Natural Science Foundation of China (Grant No. 51472069).

References

[1] Y. Fuda, K. Kumasaka, M. Katsuno, H. Sato, Y. Ino, Piezoelectric transformer for cold cathode fluorescent lamp inverter, Jpn. J. Appl. Phys. 36 (1997) 3050–3052.

[2] T.R. Gururaja, W.A. Schulze, L.E. Cross, R.E. Newnham, Piezoelectric composite materials for ultrasonic transducer applications. Part II: evaluation of ultrasonic medical applications, IEEE Trans. Son. Ultrason. 32 (1985) 499–513.

[3] R. Bermejo, H. Grünbichler, J. Kreith, C. Auer, Fracture resistance of a doped PZT ceramic for multilayer piezoelectric actuators: effect of mechanical load and temperature, J. Eur. Ceram. Soc. 30 (2010) 705–712.

[4] Y.D. Hou, M.K. Zhu, F. Gao, H. Wang, B. Wang, H. Yan, C.S. Tian, Effect of MnO_2 addition on the structure and electrical properties of $Pb(Zn_{1/3}Nb_{2/3})_{0.20}(Zr_{0.50}Ti_{0.50})_{0.80}O_3$ ceramics, J. Am. Ceram. Soc. 87 (2010) 847–850.

[5] Q.C. Wu, M.M. Hao, Z.Q. Zeng, X.C. Wang, W.Z. Lv, G.F. Fan, Nonlinear dielectric effect of Fe_2O_3-doped PMS–PZT piezoelectric ceramics for high-power applications, Ceram. Int. 43 (2017) 10866–10872.

[6] L.X. He, M. Gao, C.E. Li, W.M. Zhu, H.X. Yan, Effects of Cr_2O_3 addition on the piezoelectric properties and microstructure of $PbZr_xTi_y(Mg_{1/3}Nb_{2/3})_{1-x-y}O_3$ ceramics, J. Eur. Ceram. Soc. 21 (2001) 703–709.

[7] S.Y. Yoo, J.Y. Ha, S.J. Yoon, J.W. Choi, High-power properties of piezoelectric hard materials sintered at low temperature for multilayer ceramic actuators, J. Eur. Ceram. Soc. 33 (2013) 1769–1778.

[8] Z.G. Zhu, B.S. Li, G.R. Li, W.Z. Zhang, Q.R. Yin, Microstructure and piezoelectric properties of PMS–PZT ceramics, Mater. Sci. Eng. B 117 (2005) 216–220.

[9] J. Ryu, H.W. Kim, K. Uchino, J. Lee, Effect of Yb addition on the sintering behavior and high power piezoelectric properties of $Pb(Zr,Ti)O_3$-$Pb(Mn,Nb)O_3$, Jpn. J. Appl. Phys. 42 (2003) 1307–1310.

[10] D. Gang, R. Liang, W. Li, K. Li, W.B. Zhang, G.S. Wang, X.L. Dong, Internal bias field relaxation in poled Mn-doped $Pb(Mn_{1/3}Sb_{2/3})O_3$-$Pb(Zr,Ti)O_3$ ceramics, Ceram. Int. 39 (2013) 7703–7708.

[11] O. Ise, K. Satoh, Y. Mamiya, High power characteristics of piezoelectric ceramics in $Pb(Mn_{1/3}Nb_{2/3})O_3$-$PbTiO_3$-$PbZrO_3$ system, Jpn. J. Appl. Phys. 38 (1999) 5531–5534.

[12] H.F. Yi, R.Z. Zuo, Normal-relaxor-diffuse ferroelectric phase transition and electrical properties of $Bi(Mg_{1/2}Ti_{1/2})_3$-$PbZrO_3$-$PbTiO_3$ solid solution ceramics near the morphotropic phase boundary, J. Am. Ceram. Soc. 97 (2014) 1912–1917.

[13] R.Z. Zuo, Y. Liu, X.C. Chu, X.H. Wang, Phase transformation behavior and electrical properties of $Pb(Zr_{0.56}Ti_{0.44})O_3$-$Bi(Zn_{0.5}Ti_{0.5})O_3$ solid solution ceramics, J. Am. Ceram. Soc. 94 (2011) 4340–4344.

[14] G. Catalan, J.F. Scott, Physics and applications of bismuth ferrite, Adv. Mater. 21 (2009) 2463–2485.

[15] D. Kim, J. Yoo, I. Kim, J. Song, Dielectric and piezoelectric properties of Bi_2O_3 added (Pb,Ca,Sr)(Ti,Mn,Sb)O_3 ceramics sintered at low temperature, J. Appl. Phys. 105 (2009) (2225-2150).

[16] Y. Cheng, Y. Yang, Y.P. Wang, H.Q. Meng, Study on $Pb(Mg_{1/3}Ta_{2/3})O_3$-$Pb(Mn_{1/3}Sb_{2/3})O_3$-$Pb(Zr_xTi_{1-x})O_3$ high power piezoelectric ceramics near the morphotropic phase boundary, J. Alloy. Compd. 508 (2010) 364–369.

[17] F. Gao, L.H. Cheng, R.Z. Hong, J.J. Liu, C.J. Wang, C.S. Tian, Crystal structure and piezoelectric properties of $xPb(Mn_{1/3}Nb_{2/3})O_3$-$(0.2\text{-}x)Pb(Zn_{1/3}Nb_{2/3})O_3-0.8Pb(Zr_{0.52}Ti_{0.48})O_3$ ceramics, Ceram. Int. 35 (2009) 1719–1723.

[18] Y.K. Yan, K.H. Cho, S. Priya, Identification and effect of secondary phase in MnO_2-doped $0.8Pb(Zr_{0.52}Ti_{0.48})O_3-0.2Pb(Zn_{1/3}Nb_{2/3})O_3$ piezoelectric ceramics, J. Am. Ceram. Soc. 94 (2011) 3953–3959.

[19] X.B. Ren, Large electric-field-induced strain in ferroelectric crystals by point-defect-mediated reversible domain switching, Nat. Mater. 3 (2004) 91–94.

[20] X.B. Ren, K. Otsuka, Universal symmetry property of point defects in crystals, Phys. Rev. Lett. 85 (2000) 1016–1019.